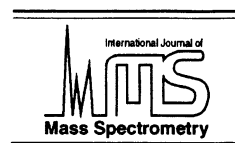




ELSEVIER

International Journal of Mass Spectrometry 195/196 (2000) 171–184



Mechanisms of reactions between ammonia and methylene oxonium ions: immonium ion formation versus transfer of the oxygen substituent

Lihn Bache-Andreassen, Einar Uggerud*

Department of Chemistry, University of Oslo, P.O. Box 1033 Blindern, N-0315 Oslo, Norway

Received 3 June 1999; accepted 8 September 1999

Abstract

Gas phase reactions of ammonia with the oxonium ions, ROCH_2^+ ($\text{R} = \text{H}, \text{CH}_3, \text{C}_2\text{H}_5, n\text{-C}_3\text{H}_7, i\text{-C}_3\text{H}_7$) have been investigated with Fourier transform ion cyclotron resonance mass spectrometry and theoretical methods (ab initio quantum chemistry, Rice-Ramsperger-Kassel-Marcus theory). In all instances two reactions are observed to occur in competition: addition/elimination, which gives $\text{CH}_2\text{NH}_2^+ + \text{ROH}$, and substitution, which gives $\text{RNH}_3^+ + \text{CH}_2\text{O}$. With the exception of $\text{R} = \text{H}$, the rate of CH_2NH_2^+ formation is by far faster than RNH_3^+ formation. The experimental observations are rationalised by the model calculations, which also show that the more exothermic the overall reaction is, the lower is the barrier. This clear trend in reactivity is dictated by the electronic properties of the R groups. For $\text{R} = i\text{-C}_3\text{H}_7$ an additional route for loss of formaldehyde was found. For the first time the prototype reaction $\text{CH}_2\text{OH}^+ + \text{NH}_3 \rightarrow \text{CH}_2\text{NH}_2^+ + \text{H}_2\text{O}$ has been observed. (Int J Mass Spectrom 195/196 (2000) 171–184) © 2000 Elsevier Science B.V.

Keywords: Ion-molecule reactions; FT-ICR; Ab initio calculations; Oxonium ions; Nucleophilic substitution; Addition-elimination; Imines

1. Introduction

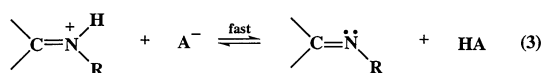
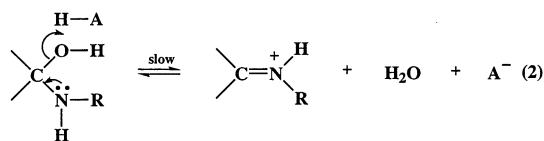
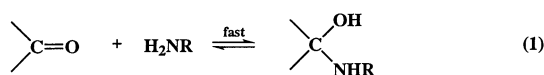
Aldehydes and ketones react with amines to give imines (Schiff bases) [1–3]. The formation of imines has been studied extensively, and the mechanism is rather well understood in the liquid phase [4,5]. Briefly, the reaction is general acid catalysed, with a maximum rate around $\text{pH} = 4$, and it has been postulated to occur via the key steps shown in Scheme 1. As indicated in Scheme 1, the central step in this addition/elimination

(ae) mechanism is proton transfer from the general acid to the oxygen atom and it is rate determining.

A fundamental issue in all mechanistic studies is how reactivity depends on the intrinsic properties of the reacting molecules. This information is available from gas phase studies. By systematic examination of suitable model systems in the gas phase it is possible to gain insight into the factors which govern liquid phase reactivity. Several workers have found that immonium ions are formed in chemical ionization mass spectrometry by water loss from adducts between amines and a number of protonated carbonyl compounds [6–8]. These studies were, however, not sufficiently specific to determine the mechanism of immonium formation. Vainiotalo and co-workers [9]

* Corresponding author. E-mail: enar.uggerud@kjemi.uio.no

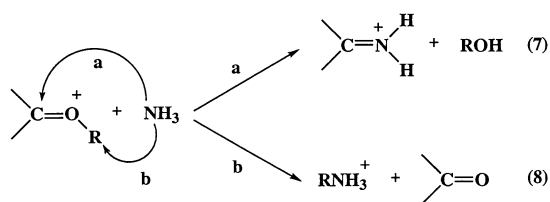
Dedicated to Bob Squires for his many seminal contributions to mass spectrometry and ion chemistry.



Scheme 1.

investigated the reaction between protonated acetone and amines at very low pressures ($p = 10^{-8}$ mbar, Fourier transform ion cyclotron resonance mass spectrometer), as shown in Scheme 2, but did not observe formation of the protonated imine [reaction (4)]. Instead, proton transfer to the more basic amine [reaction (5)] was observed. However, when the otherwise easily transferable proton of protonated acetone is blocked by a second acetone molecule, thereby forming a protonated acetone dimer, reaction with an amine gave the anticipated protonated imine [reaction (6)].

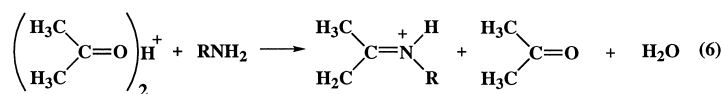
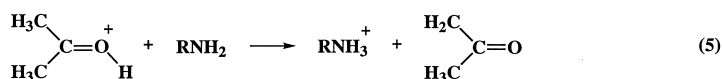
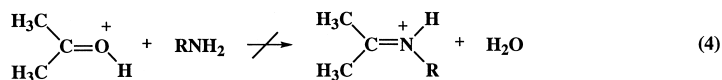
When the proton of the protonated carbonyl compound is substituted by an alkyl group the addition/elimination (**ae**) route is the preferred reaction [reaction (7)]. This has been noticed by several authors [10–12]. Transfer of the alkyl group to the amine, which for $\text{R} \neq \text{H}$ formally corresponds to a nucleophilic substitution reaction (**sub**), is also observed [reaction (8)], but is of significantly lower abundance.



Scheme 3.

This ambident character of alkyl oxonium ions has also been observed in reactions with alcohols, ethers, aldehydes, ketones and other classes of organic compounds [10,13–30]. The general principles of gas phase **ae** reactions have been investigated and discussed in an earlier paper by us [31]. A common feature among gas phase **ae** reactions, which distinguishes them from their solution counterparts, is that they involve intramolecular 1,3-proton transfer between the initial nucleophilic addition and eventual elimination.

As already mentioned an oxonium ion has two electrophilic centres. This is indicated in Scheme 3. A closer mechanistic analysis reveals that the two pathways (addition/elimination—path a, or substitution—path b) differ by the fact that the nucleophile initially attacks the oxonium ion. So far, no systematic investigation of the factors which determine the product distribution in reactions between oxonium ions and a nucleophile has been done. It is of great interest to learn more about how the electronic structure of the oxonium ion and the attractive interactions between the oxonium ion and the incoming nucleophile may influence the outcome of the reaction. It is therefore interesting to see how the nature of the R substituents



Scheme 2.

may come into play. In this article we present results for reactions between oxonium ions of the type $^+\text{CH}_2\text{OR}$ ($\text{R} = \text{H}, \text{CH}_3, \text{C}_2\text{H}_5, n\text{-C}_3\text{H}_7, i\text{-C}_3\text{H}_7$) and ammonia. Our study is based on kinetic measurements of the reactions in the cell of a Fourier transform ion cyclotron resonance (FTICR) mass spectrometer and extensive ab initio quantum chemical calculations of relevant stationary points along the reaction paths.

2. Experimental and theoretical methods

2.1. Mass spectrometric experiments

The reactions were studied with a FTICR mass spectrometer equipped with an external ion source (Apex 47 e, Bruker Daltonics, Billerica, MA, USA). The appropriate reactant ions (ROCH_2^+) were formed by 70 eV electron impact on a suitable ether ($\text{ROCH}_2\text{R}'$) in the external ion source. The mixture of ions produced in this way were transferred to the ICR cell which contained NH_3 (or ND_3) at a stationary partial pressure of typically 1×10^{-8} mbar. The temperature of the cell was estimated to be approximately 300 K. All ions with m/z values different from that of the ion of interest (ROCH_2^+) were then ejected from the cell by correlated frequency sweep [32]. Subsequent to this argon was introduced to the cell via a pulsed valve (peak pressure 10^{-5} mbar) and then allowed to pump away for 3–4 s. During this period multiple collisions between the trapped ions and argon ensured that the ions were thermally and translationally cooled to ambient conditions before they were brought to reaction. After this event complete isolation of the ROCH_2^+ ions was accomplished by single frequency shots to get rid of unwanted ions. This was necessary because small amounts of ionic reaction products and fragment ions formed by collisionally induced decomposition are formed during the cooling period. The reactions were observed by recording mass spectra after a variable reaction time, t_r . In this way the product ion distribution could be obtained as a function of time. Pseudo-first-order rate constants for the total consumption of the reactant ions (k_{tot}) were taken from the slope of the straight line obtained by plotting the logarithm of the normalised reactant ion intensities against t_r . The

high degree of linearity of the plots demonstrated that the reactant ions were translationally and thermally equilibrated as the result of their careful preparation. To obtain the rate constants for formation of the two primary products ($k_{\text{sub}} + k_{\text{ae}} = k_{\text{tot}}$) the relative intensity of the addition/elimination product was plotted against the intensity of the substitution product (all secondary products included). Great care was taken to ensure linearity of this plot, and the slope of the plot was taken to be the ratio $k_{\text{ae}}/k_{\text{sub}}$. All measurements were repeated in at least four different sessions to ensure long time reproducibility and to obtain reliable measurement statistics. The ion gauge was calibrated by measurement of the reaction $\text{NH}_3^+ + \text{NH}_3 \rightarrow \text{NH}_4^+ + \text{NH}_2$ ($k = 2.2 \times 10^{-9} \text{ cm}^3 \text{ molecule}^{-1} \text{ s}^{-1}$) [33]. The instrument was operated at sufficiently high resolution to identify all reactants and products by precise mass measurement. Chemicals were of research quality and checked for purity by mass spectrometry. Reaction efficiencies were estimated using collisional rates obtained by the parametrised model of Su and Chesnavich [34].

2.2. Quantum chemical model calculations

Quantum chemical calculations were carried out using the program systems GAUSSIAN 94 [35]. The basis sets 3-21G and 6-31G(d, p) was employed [36]. The quantum chemical methods used were Hartree-Fock (HF) [37], Møller-Plesset perturbation theory to second order (MP2) [38], and the compound G2 method [39].

All relevant critical points (reactants, transition structures, intermediates, and products) of the potential energy surface were characterised by complete optimisation of the molecular geometries for HF/3-21G, MP2/6-31G(d, p), and G2. Owing to unacceptable demands on computer resources G2 calculations were not carried out for $\text{R} = \text{C}_3\text{H}_7$. Harmonic frequencies were obtained by diagonalising the mass-weighted Cartesian force constant matrix, calculated from the analytical second derivatives of the total energy (the Hessian). Harmonic frequencies obtained in this manner were used to calculate the zero point vibrational energies (ZPVE) as described in the following. Relative energies were calculated by including the MP2/6-31G(d, p) zero point vibrational energies

Table 1
Experimental rate constants

R	k_{ae}^a	k_{sub}^a	$f^b = k_{ae}/k_{sub}$	$\Sigma k^a =$ $k_{ae} + k_{sub}$	γ_{ae}^c	γ_{sub}^c	$\Sigma \gamma^c = \gamma_{ae} + \gamma_{sub}$
–H	0.061	6.1	0.010	6.2	0.0026	0.26	0.26
–CH ₃	2.7	0.25	10.8	3.0	0.12	0.011	0.13
–C ₂ H ₅	3.0	0.016	188	3.0	0.14	0.000 74	0.14
–CH(CH ₃) ₂	2.2	0.014	157	2.2	0.10	0.000 66	0.10
–CH ₂ CH ₂ CH ₃	2.7	0.014	193	2.7	0.13	0.000 66	0.13

^a All the rate constants are given in units of $10^{-10} \text{ cm}^3 \text{ molecule}^{-1} \text{ s}^{-1}$. The uncertainty in the experimental rate constants is estimated to be around 25%.

^b The uncertainty in the relative rate constants is estimated to be around 5%.

^c The reaction efficiency, γ , is calculated as the ratio between the experimental reaction rate constant and the collision rate constant. The collision rate constant is calculated using parameterised trajectory theory, see text for details.

scaled by a factor of 0.9608 [MP2/6-31G(*d, p*)] [40]. For the G2 method [39] the built-in scale factor was used.

2.3. Rice-Ramsperger-Kassel-Marcus calculations [41]

A standard computer procedure was employed. The scaled normal frequencies of vibration from the MP2/6-31G(*d, p*) calculations were used as input. Details of the calculations (list of frequencies etc.) may be obtained from the authors upon request.

3. Experimental results

For all five systems studied the following two reactions were observed to occur in competition:



The results are given in Table 1. The reader should note that the uncertainty in our reported absolute rate constants generally is $\pm 25\%$, mainly as a result of the precision in the pressure gauge reading. However, within the series of measurements presented here the uncertainty in the product distribution factors (relative rate constants) is only $\pm 5\%$.

For R = H proton transfer [reaction (10)] is dominating. Our rate constant of $k_{sub}(\text{H}) = 6.1 \times 10^{-10}$

$\text{cm}^3 \text{ molecule}^{-1} \text{ s}^{-1}$ agrees well with previous measurements of Okada et al. ($8.0 \times 10^{-10} \text{ cm}^3 \text{ molecule}^{-1} \text{ s}^{-1}$) [11] and Matsumoto et al. ($8.6 \times 10^{-10} \text{ cm}^3 \text{ molecule}^{-1} \text{ s}^{-1}$) [42]. Apparently because our measurements were conducted over a longer reaction period than those of Okada et al. and Matsumoto et al., we were able to observe the addition/elimination product, CH_2NH_2^+ . The rate is $k_{ae}(\text{H}) = 6.1 \times 10^{-12} \text{ cm}^3 \text{ molecule}^{-1} \text{ s}^{-1}$, which is 1% of the rate of the proton transfer reaction. This finding is quite extraordinary because it represents the first observation of the simplest possible (R = H) system where this type of addition/elimination can occur. Moreover, the fact that this reaction takes place must be of significance to interstellar chemistry, because ammonia, formaldehyde, methylene imine, and water are known to be abundant in interstellar clouds [43,44].

For R = CH₃ the addition/elimination pathway takes over, and methyl group transfer (nucleophilic substitution) only accounts for about 10%. Our rate constants [$k_{ae}(\text{CH}_3) = 2.7 \times 10^{-10} \text{ cm}^3 \text{ molecule}^{-1} \text{ s}^{-1}$ and $k_{sub}(\text{CH}_3) = 2.5 \times 10^{-11} \text{ cm}^3 \text{ molecule}^{-1} \text{ s}^{-1}$] are in reasonable agreement with previous measurements of Okada et al. [11] [$k_{ae}(\text{CH}_3) = 1.3 \times 10^{-10} \text{ cm}^3 \text{ molecule}^{-1} \text{ s}^{-1}$ and $k_{sub}(\text{CH}_3) = 3.7 \times 10^{-11} \text{ cm}^3 \text{ molecule}^{-1} \text{ s}^{-1}$], with Freitas and O'Hair [22] [$k_{ae}(\text{CH}_3) = 5.9 \times 10^{-10} \text{ cm}^3 \text{ molecule}^{-1} \text{ s}^{-1}$], and with Wilson et al. [28] [ICR: $k_{ae}(\text{CH}_3) = 4.3 \times 10^{-10} \text{ cm}^3 \text{ molecule}^{-1} \text{ s}^{-1}$, selected ion flow tube (SIFT): $k_{ae}(\text{CH}_3) = 5.9 \times 10^{-10} \text{ cm}^3 \text{ molecule}^{-1} \text{ s}^{-1}$]. At long reaction times NH_4^+ is observed. Okada

et al. [11] suggested that this ionic species was formed as the result of



They suggested that the neutral product is ethylene oxide (oxirane). We have good reason to disregard their suggestion, and propose an alternative explanation. The methylene immonium ions produced in reaction (9) reside in the FT-ICR cell, and during reaction a large concentration build up. The ions react further by proton transfer according to:



A separate experiment was carried out with the isolated CH_2NH_2^+ product of electron ionization (EI) of hexylamine. It was demonstrated that the rate of the proton transfer of reaction (12) was $k_{12} = 1.9 \times 10^{-12} \text{ cm}^3 \text{ molecule}^{-1} \text{ s}^{-1}$, and kinetic modeling of the reaction manifold fits well with the found temporal NH_4^+ distribution.

Addition/elimination is also dominating when $\text{R} = \text{C}_2\text{H}_5$, $n\text{-C}_3\text{H}_7$, $i\text{-C}_3\text{H}_7$, and the proportion of addition/elimination to substitution for these larger substituents are significantly smaller than for $\text{R} = \text{CH}_3$ (Table 1).

For $\text{R} = \text{C}_2\text{H}_5$ we performed an additional experiment using ND_3 instead of NH_3 . We determined an intermolecular isotope effect of $k_{\text{H}}/k_{\text{D}} = 1.4$ for the addition/elimination reaction and $k_{\text{H}}/k_{\text{D}} = 1.0$ for the substitution reaction. The significance of these findings will be discussed in Sec. 4.

4. Quantum chemical models

A systematic study of the stationary points of the reaction paths for the competing addition/elimination and substitution reactions was conducted for all five systems under investigation and the results are presented in Table 2. For each species only data for the rotamer with the lowest potential energy are reported. Fig. 1 shows the general potential energy profiles for the two mechanisms, and defines the energy parameters used in the discussion. The geometries of the species involved are displayed in Fig. 2 and Table 3. The relative potential energies (MP2 and G2 values including ZPVE)

of the stationary structures along the reaction paths (see Fig. 1 for definition of all quantities) are given in Table 4. The MP2 data will be discussed here.

4.1. Addition/elimination mechanism (ae)

The mechanism for immonium ion formation is similar for all five substituents. An initial nucleophilic attack of ammonia on the methylene carbon leads to formation of a N-protonated carbinolamine as the first intermediate. This isomerises to the second intermediate, the corresponding O-protonated carbinolamine, by intramolecular proton transfer. This intramolecular proton transfer constitutes a tight transition state, and is the rate limiting step of the mechanism, as evident by the experimentally observed isotope effect of $k_{\text{H}}/k_{\text{D}} = 1.4$. Subsequent to the intramolecular proton transfer the ROH entity is lost and the final product ion, CH_2NH_2^+ , is formed. The thermochemical driving force is the formation of a strong C=N bond.

Our theoretical models are in good qualitative agreement with those of Bouchoux and Hoppilard [45] for $\text{R} = \text{H}$, except that these authors did not locate the central transition structure. There is also good agreement with Okada et al. [11] and with Freitas and O'Hair [22] for $\text{R} = \text{CH}_3$. Bouchoux and Hoppilard [45] and Okada et al. [11] employed simpler wave functions than those used here, whereas Freitas and O'Hair [22] used a wave function of a similar kind as we did.

When we compare the results we observe clear trends in the energetics of the reactants, intermediates, transition structures, and products with the nature of the substituent, R. We have recently introduced a set of generally applicable stabilisation constants for different R groups to express their ability—as cations—to accept a Lewis base [46]. The constants are $a = 1.000, 0.938, 0.915$, and 0.895 for $\text{R} = \text{H}, \text{CH}_3, \text{C}_2\text{H}_5$, and $i\text{-C}_3\text{H}_7$, respectively, and will be used to anchor the present data. We term the energy difference between the reactants ($\text{NH}_3 + \text{ROCH}_2^+$) and the first and second intermediates, respectively, as $E_{\text{ac}}(\text{Int1})$ and $E_{\text{ac}}(\text{Int2})$, see Fig. 1. The energy difference between the reactants and the transition structure for the proton transfer is $E_{\text{ac}}(\text{TS})$, and $E_{\text{ac}}(\text{Prod})$ is the energy difference between the reactants and the products. With these

Table 2
Absolute energies

Molecule	HF/3-21G (Hartree) ^a	MP2/6-31G(<i>d, p</i>) (Hartree) ^a	G2(0 K) (Hartree) ^a
NH ₃ (1)	-55.839 03	-56.349 13	-56.458 65
CH ₂ OH ⁺ (2a)	-113.474 94	-114.429 61	-114.607 76
NH ₃ ···CH ₂ OH ⁺ (3a)	-169.410 35	-170.863 77	-171.144 16
H-TS (ae) (4a)	-169.366 69	-170.817 44	-171.094 74
NH ₂ CH ₂ ···OH ₂ ⁺ (5a)	-169.407 37	-170.859 34	-171.142 31
CH ₂ NH ₂ ⁺ (6)	-93.809 27	-94.638 10	-94.791 84
H ₂ O (7a)	-75.565 91	-76.198 76	-76.332 05
CH ₂ O···HNH ₃ ⁺ (10a)	-169.421 86	-170.873 01	-171.150 45
NH ₄ ⁺ (11a)	-56.185 45	-56.684 78	-56.781 40
CH ₂ O (12)	-113.195 14	-114.157 18	-114.338 92
CH ₂ OCH ₃ ⁺ (2b)	-152.283 60	-153.590 17	-153.840 39
NH ₃ ···CH ₂ OCH ₃ ⁺ (3b)	-208.200 61	-210.007 15	-210.359 55
CH ₃ -TS (ae) (4b)	-208.162 20	-209.967 42	-210.316 39
NH ₂ CH ₂ ···OHCH ₃ ⁺ (5b)	-208.192 83	-209.993 99	-210.348 86
CH ₃ OH (7b)	-114.347 85	-115.331 12	-115.534 90
NH ₃ ···CH ₃ OCH ₂ ⁺ (8b)	-208.145 47	-209.959 37	-210.314 64
CH ₃ -TS (sub) (9b)	-208.144 67	-209.953 88	-210.307 52
CH ₂ O···CH ₃ NH ₃ ⁺ (10b)	-208.195 77	-210.009 72	-210.361 61
CH ₃ NH ₃ ⁺ (11b)	-94.981 69	-95.838 05	-96.007 75
CH ₂ OCH ₂ CH ₃ ⁺ (2c)	-191.086 56	-192.755 90	-193.077 29
NH ₃ ···CH ₂ OCH ₂ CH ₃ ⁺ (3c)	-246.998 43	-249.168 11	-249.591 61
CH ₃ CH ₂ -TS (ae) (4c)	-246.960 94	-249.130 20	-249.580 13
NH ₂ CH ₂ ···OHCH ₂ CH ₃ ⁺ (5c)	-246.991 95	-249.154 28	-249.580 13
CH ₃ CH ₂ OH (7c)	-153.144 36	-154.490 09	-154.764 27
NH ₃ ···CH ₃ CH ₂ OCH ₂ ⁺ (8c)	-246.945 01	-249.122 67	-249.549 70
CH ₃ CH ₂ -TS (sub) (9c)	-246.940 96	-249.112 70	-249.539 20
CH ₂ OCH ₂ CH ₃ ···NH ₃ ⁺ (10c)	-246.994 50	-249.171 23	-249.593 78
CH ₂ CH ₃ NH ₃ ⁺ (11c)	-133.780 57	-134.999 29	-135.240 43
CH ₂ OCH(CH ₃) ₂ ⁺ (2d)	-229.890 07	-231.923 09	-232.315 56
NH ₃ ···CH ₂ OCH(CH ₃) ₂ ⁺ (3d)	-285.795 93	-288.330 54	...
(CH ₃) ₂ CH-TS (ae) (4d)	-285.760 28	-288.294 36	...
NH ₂ CH ₂ ···OHCH(CH ₃) ₂ ⁺ (5d)	-285.790 91	-288.316 38	...
(CH ₃) ₂ CHOH (7d)	-191.942 06	-193.650 72	-193.996 46
NH ₃ ···(CH ₃) ₂ CHOCH ₂ ⁺ (8d)	-285.746 60	-288.287 39	...
(CH ₃) ₂ CH-TS (sub) (9d)	-285.739 54	-288.275 45	...
CH ₂ OCH(CH ₃) ₂ ···NH ₃ ⁺ (10d)	-285.794 02	-288.334 90	...
(CH ₃) ₂ CHNH ₃ ⁺ (11d)	-172.580 43	-174.162 44	-174.475 02
NH ₃ ···H-C ₃ H ₆ OCH ₂ ⁺ (13d)	...	-288.287 39	...
(CH ₃) ₂ CH-TS (elim) (14d)	...	-288.273 19	...
NH ₃ -H···C ₃ H ₆ ···OCH ₂ ⁺ (15d)	...	-288.315 91	...
NH ₃ -H···C ₃ H ₆ ⁺ (16d)	...	-174.130 84	...
CH ₂ OCH ₂ CH ₂ CH ₃ ⁺ (2e)	-229.880 12	-231.912 06	-232.305 28
NH ₃ ···CH ₂ OCH ₂ CH ₂ CH ₃ ⁺ (3e)	-285.789 72	-288.322 80	...
CH ₃ CH ₂ CH ₂ -TS (ae) (4e)	-285.753 24	-288.285 11	...
NH ₂ CH ₂ ···OHCH ₂ CH ₂ CH ₃ ⁺ (5e)	-285.783 97	-288.308 98	...
CH ₃ CH ₂ CH ₂ OH (7e)	-191.936 98	-193.643 99	-193.989 21
NH ₃ ···CH ₃ CH ₂ CH ₂ OCH ₂ ⁺ (9e)	-285.738 00	-288.278 49	...
CH ₃ CH ₂ CH ₂ -TS (sub) (10e)	-285.733 83	-288.268 40	...
CH ₂ O···CH ₃ CH ₂ CH ₂ NH ₃ ⁺ (11e)	-285.786 88	-288.326 35	...
CH ₃ CH ₂ CH ₂ NH ₃ ⁺ (12e)	-172.573 79	-174.154 75	-174.467 55

^a Zero-point vibrational energy scaled by 0.9207 (HF/3-21G) and 0.9608 [MP2/6-31G(*d, p*)] are included in all the energies. For the G2 calculations the built-in scale factor was used.

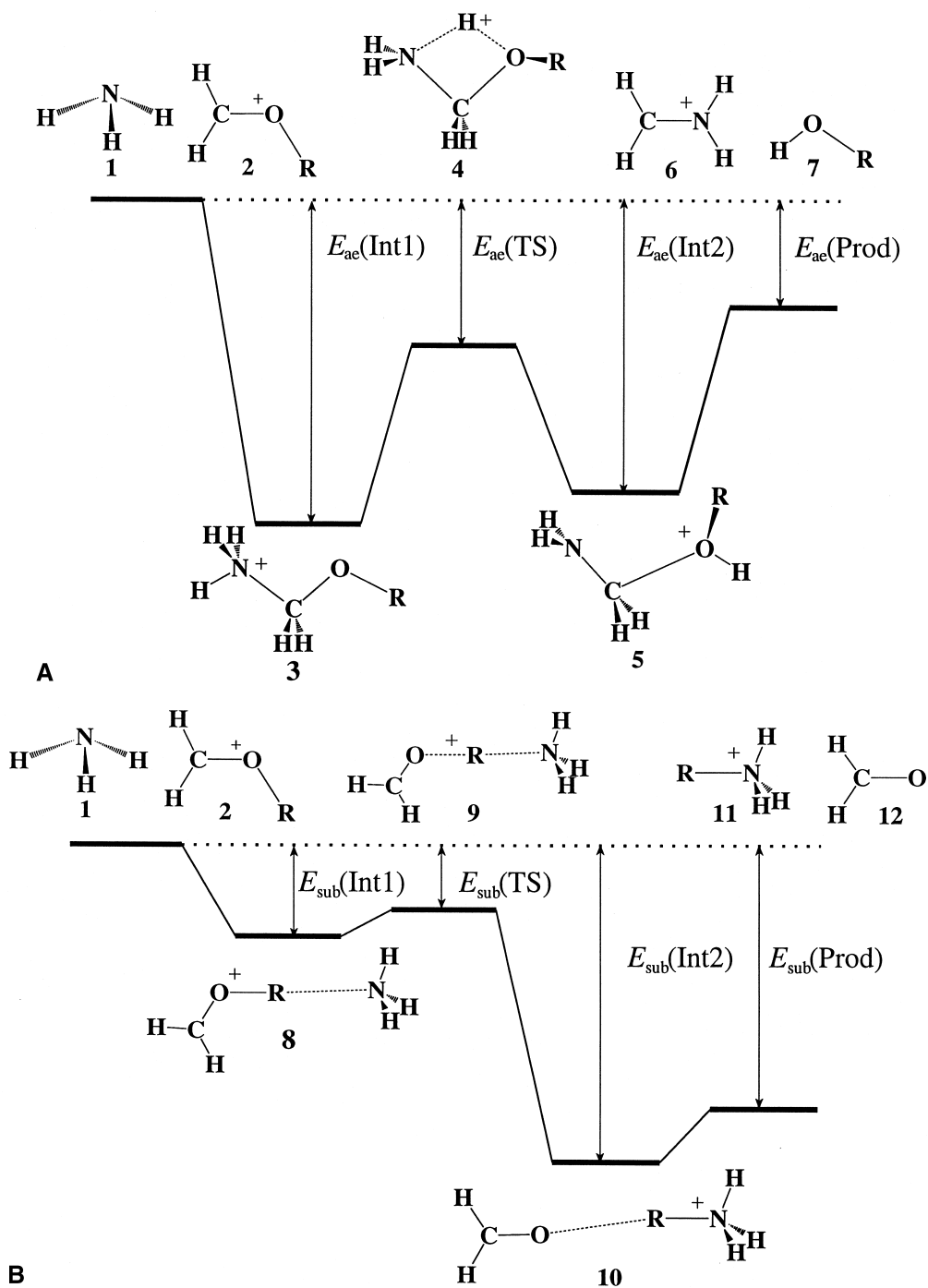


Fig. 1. Schematic potential energy diagram for (a) the addition/elimination (ae) mechanism, (b) the substitution (sub) mechanism. See Table 4 for the actual values of the indicated energy parameters.

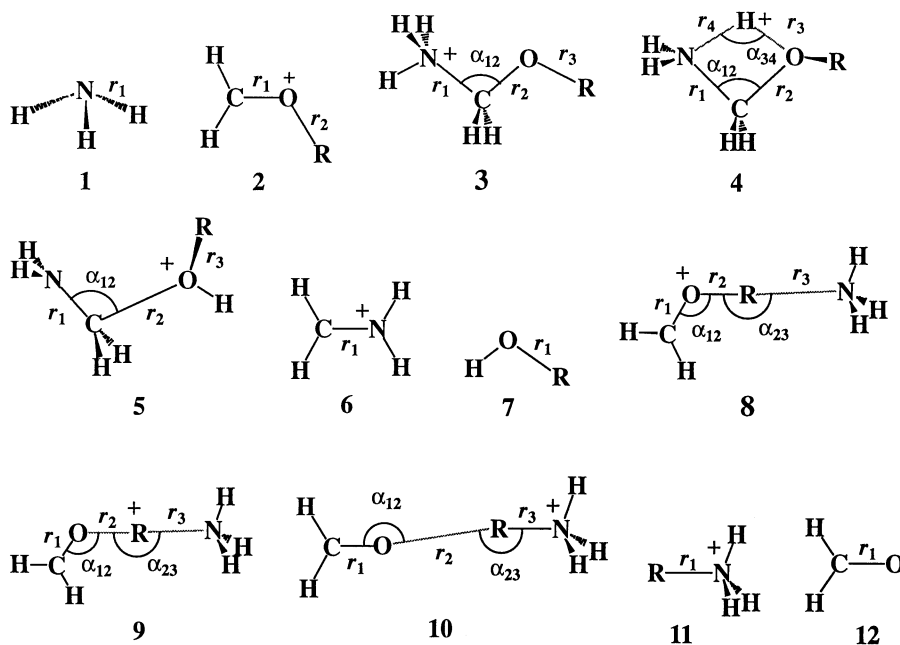


Fig. 2. Structures of the stationary points with indication of the most important geometrical parameters. See Table 3 for the actual values.

definitions all quantities have positive signs. It would be interesting to see how the electronic structures of the system responds to the properties of the substituents ($R = \text{H}, \text{CH}_3, \text{C}_2\text{H}_5, i\text{-C}_3\text{H}_7$). It turned out that there is a linear relationship between the relative energies of all stationary points and the a constants (all quantities are in kJ mol^{-1} and the goodness-of-fit parameter of the linear plot, r , is given for each):

$$E_{\text{ae}}(\text{Int1}) = 685a - 463, \quad r = 0.998 \quad (13)$$

$$E_{\text{ae}}(\text{TS}) = 415a - 314, \quad r = 0.997 \quad (14)$$

$$E_{\text{ae}}(\text{Int2}) = 927a - 718, \quad r = 0.999 \quad (15)$$

$$E_{\text{ae}}(\text{Prod}) = 1049a - 899, \quad r = 0.989 \quad (16)$$

The fact that the barrier height decreases [$E_{\text{ae}}(\text{TS})$ increases] when the overall reaction becomes more exothermic is evident from this analysis. When we look more closely at the central chemical transformation, $\text{Int1}(3) \rightarrow \text{Int2}(5)$ [Fig. 1(a), Table 4], we notice that this reaction step becomes more and more endothermic [$E_{\text{ae}}(\text{Int1}) - E_{\text{ae}}(\text{Int2})$ increases] along the line $R = \text{H}, \text{CH}_3, \text{C}_2\text{H}_5$, and $i\text{-C}_3\text{H}_7$. Simultaneous to this both the forward [$E_{\text{ae}}(\text{Int1}) - E_{\text{ae}}(\text{TS})$] and the reverse barrier [$E_{\text{ae}}(\text{Int2}) - E_{\text{ae}}(\text{TS})$] decrease. At first sight this seems

unusual and is in apparent conflict with the extended Hammond postulate [47], which predicts that the forward barrier should increase and the reverse barrier should decrease. Inspection of the geometrical data (Fig. 2, Table 3) is also confusing, because there is no correlation between the anticipated position of the TS along the reaction coordinate, and the lengths of the bond being broken (r_4) and the bond (r_3) being formed. However, all this confusion is resolved by realizing that the intramolecular proton transfer involves a rather intricate electronic reorganization where more than one bond is broken and more than one is formed [31]. Accompanying proton transfer from N to O, there is a significant shortening of the C–N bond from a single to a double bond and a simultaneous lengthening of the C–O bond from a double to a single bond. For this reason the so-called adiabatic criterion of the Hammond postulate is not valid [47].

Because the stabilisation constant, a —according to our definition—is not defined for $R = n\text{-C}_3\text{H}_7$, the data for this system has been omitted from the analysis. It is also a problem that the normal propyl group may rearrange to the more stable isopropyl

Table 3

Geometries for the structures shown in Fig. 2; all the bond lengths are in angstroms, and all angles are in degrees

Structure		–H (a)	–CH ₃ (b)	–CH ₂ CH ₃ (c)	–CH(CH ₃) ₂ (d)	–CH ₂ CH ₂ CH ₃ (e)
CH ₂ OR ⁺ (2)	<i>r</i> ₁	1.252	1.249	1.248	1.247	1.248
	<i>r</i> ₂	0.983	1.494	1.528	1.551	1.520
NH ₃ ⋯CH ₂ OR ⁺ (3)	<i>r</i> ₁	1.505	1.507	1.508	1.547	1.551
	<i>r</i> ₂	1.388	1.381	1.380	1.363	1.361
	<i>r</i> ₃	0.967	1.446	1.457	1.472	1.460
	α ₁₂	101.4	102.1	102.2	107.7	108.0
R–TS (ae) (4)	<i>r</i> ₁	1.458	1.463	1.466	1.464	1.467
	<i>r</i> ₂	1.493	1.477	1.474	1.471	1.473
	<i>r</i> ₃	1.177	1.200	1.210	1.216	1.212
	<i>r</i> ₄	1.399	1.365	1.354	1.347	1.352
	α ₁₂	93.4	93.2	93.4	93.4	93.4
	α ₃₄	112.7	112.7	113.0	113.1	113.1
NH ₂ CH ₂ ⋯OHR ⁺ (5)	<i>r</i> ₁	1.284	1.288	1.290	1.294	1.292
	<i>r</i> ₂	2.404	2.271	2.214	2.147	2.173
	<i>r</i> ₃	0.965	1.441	1.456	1.467	1.454
	α ₁₂	110.1	108.2	108.3	108.3	107.5
ROH (7)	<i>r</i> ₁	0.961	1.421	1.426	1.431	1.427
NH ₃ ⋯ROCH ₂ ⁺ (8)	<i>r</i> ₁	⋯	1.246	1.246	1.245	1.246
	<i>r</i> ₂	⋯	1.528	1.542	1.569	1.538
	<i>r</i> ₃	⋯	2.724	2.943	3.143	2.957
	α ₁₂	⋯	121.1	120.9	123.8	120.6
	α ₂₃	⋯	178.4	160.3	145.8	160.1
	R–TS (sub) (9)	<i>r</i> ₁	⋯	1.239	1.237	1.235
	<i>r</i> ₂	⋯	1.775	1.857	1.967	1.858
	<i>r</i> ₃	⋯	2.205	2.258	2.355	2.263
	α ₁₂	⋯	120.7	120.4	120.4	120.4
	α ₂₃	⋯	177.7	167.3	162.1	167.4
CH ₂ O⋯RNH ₃ ⁺ (10)	<i>r</i> ₁	1.230	1.225	1.226	1.226	1.226
	<i>r</i> ₂	1.667	2.756	2.893	2.965	2.909
	<i>r</i> ₃	1.053	1.511	1.521	1.529	1.520
	α ₁₂	139.6	173.7	176.6	177.9	176.9
	α ₂₃	166.5	172.2	158.2	152.7	157.0
RNH ₃ ⁺ (11)	<i>r</i> ₁	1.023	1.507	1.518	1.528	1.518
NH ₃ (1)	<i>r</i> ₁	1.013				
CH ₂ NH ₂ ⁺ (6)	<i>r</i> ₁	1.282				
CH ₂ O (12)	<i>r</i> ₁	1.220				

group at some stage along the reaction trajectory, with the consequence that a comparison between theory and experiment would be obscure. It is, however, informative that the data for R = *n*-C₃H₇ fit well in between those for R = C₂H₅ and *i*-C₃H₇.

4.2. S_N2 mechanisms (*sub*)

For R ≠ H the transfer of an alkyl group from formaldehyde to ammonia corresponds to an S_N2 reaction. The thermochemical driving force is the larger

Table 4

Relative potential energies for substitution and addition–elimination mechanisms on the MP2/6-31G(d, p) and G2 level; the quantities are defined in Fig. 1; all values are in kilojoule per mole

R	$E_{ae}(\text{Int1})$	$E_{ae}(\text{TS})$	$E_{ae}(\text{Int2})$	$E_{ae}(\text{Prod})$	$E_{sub}(\text{Int1})$	$E_{sub}(\text{TS})$	$E_{sub}(\text{Int2})$	$E_{sub}(\text{Prod})$
–H (MP2)	223.3	101.6	211.6	152.6	247.5	166.0
–CH ₃ (MP2)	178.1	73.8	143.6	78.5	52.7	38.3	184.9	146.8
–CH ₂ CH ₃ (MP2)	165.6	66.1	129.3	60.8	46.3	20.1	173.8	135.0
–CH(CH ₃) ₂ (MP2)	153.1	58.1	115.9	43.6	39.8	8.5	164.6	124.5
–CH ₂ CH ₂ CH ₃ (MP2)	161.7	62.8	125.5	54.9	45.4	18.9	171.1	133.2
–H (G2)	204.2	74.4	199.3	151.0	220.7	141.6
–CH ₃ (G2)	158.9	45.6	130.8	72.8	41.0	22.3	164.3	125.1
–CH ₂ CH ₃ (G2)	146.2	37.9	116.0	53.0	36.1	8.6	151.9	114.0

alkyl cation affinity of ammonia compared to formaldehyde, and also in this case the barrier becomes lower the more exothermic the reaction is. These features are evident from the reaction diagram of Fig. 1(b) and Table 4. In the case of R = H, the mechanism reduces to a single minimum proton transfer from formaldehyde to the more basic ammonia. The energy differences (for R = CH₃, C₂H₅, *i*-C₃H₇) show a linear dependence on the electronic property of the R group as already discussed for the **ae** mechanism:

$$E_{sub}(\text{Int1}) = 300a - 228; \quad r = 0.998 \quad (17)$$

$$E_{sub}(\text{TS}) = 696a - 615; \quad r = 0.992 \quad (18)$$

$$E_{sub}(\text{Int2}) = 472a - 258; \quad r = 1.000 \quad (19)$$

$$E_{sub}(\text{Prod}) = 519a - 340; \quad r = 1.000 \quad (20)$$

The transition structures (**9**) for the **sub** mechanism (Fig. 2, Table 3) are typical for S_N2 reactions. The factors that govern the stabilities of transition structures of S_N2 reactions relative to reactants have been discussed by us in an earlier article [48]. Also in this case the most exothermic overall reaction gives the lowest energy transition structure. For the actual chemical transformation, Int1(**8**) → Int2(**10**) [Fig. 1(b), Table 4], the situation is again less clear. The correlation between the position of the TS along the reaction coordinate (expressed by r_2 or r_3 , Table 3) and the forward barrier [$E_{sub}(\text{Int1}) - E_{sub}(\text{Int2})$, Table 4], is as one should expect from the Hammond postulate: for an exothermic step a lower barrier will give a more reactant like TS. However, both the forward and the reverse barriers increase with de-

creasing exothermicity—in disagreement with the Hammond postulate prediction. The problem is most likely that the electronic reorganization also could involve the C=O partial double bond in addition to the bonds being directly formed and broken.

5. Discussion

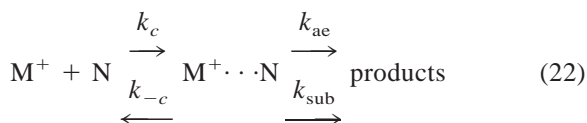
From the data of Table 4 with reference to the potential energy diagram of Fig. 1 it is easy to understand why proton transfer dominates over immonium ion formation for R = H. The proton transfer (**sub**) has no transition structure in this particular case, and has a loose transition state. The competing **ae** reaction has both a higher barrier and a tight transition state.

The rate constant for immonium ion formation relative to R-group transfer is expressed by the product distribution factor $f = k_{ae}/k_{sub}$ (Table 1). Along the series R = CH₃, C₂H₅, *i*-C₃H₇ the experimentally determined ratio increases from CH₃ to C₂H₅. From C₂H₅ to *i*-C₃H₇ the ratio f decreases nominally, which we judge to be significant because the precision in the relative rate constants is better than ±5%. The quantum chemical models predict that the difference in the barrier heights for **ae** and **sub** increases continuously along the series R = CH₃, C₂H₅, *i*-C₃H₇. This does not necessarily imply that f should increase too. To get some insight into this, we performed approximate Rice-Ramsperger-Kassel-Marcus (RRKM) calculations to investigate the cumulative effect of (1). The difference in barriers for **ae** and **sub** [$E_{ae}(\text{TS}) - E_{sub}(\text{TS})$], (2). the potential energy

of the transition structures relative to the reactants [$E_{\text{ae}}(\text{TS})$ and $E_{\text{sub}}(\text{TS})$], and (3). the number of degrees of freedom. The RRKM expression [41] for the rate coefficient is

$$k(E) = \frac{G^*(E - E_0)}{hN(E)} \quad (21)$$

where E is the energy, E_0 is the critical energy of the reaction, G^* is the integrated density of states at the transition state, h is Planck's constant, and N is the density of states of the reacting species. The outcome of an ion–molecule encounter with a given bimolecular rate constant for the association, k_c , may either be resultless (backdissociation to reactants, with a given unimolecular rate constant k_{-c}), or the chemical transformations may take place, with given unimolecular rate constants k_{ae} and k_{sub} :



The problem was simplified by assuming that both chemical transformation take place via the same intermediate $\text{M}^+ \cdots \text{N}$, which was taken to be the $\text{H}_3\text{N}-\text{CH}_2-\text{OR}^+$ species (**3**) of the **ae** mechanism. This is the lowest energy intermediate, and it seems reasonable to assume that the interconversion between this intermediate and (**8**) of the **sub** mechanism is fast and reversible. The effect of rotation (J quantum number) was neglected in our treatment. The MP2/6-31G(d, p) energies and scaled frequencies were used, and available translational, rotational, and vibrational energies corresponding to a temperature of 298 K was added to the reacting molecules. It was assumed that the steady state approximation is valid for the intermediate $\text{H}_3\text{N}-\text{CH}_2-\text{OR}^+$ at any given energy, i.e. $d[\text{M}^+ \cdots \text{N}]/dt = 0$. Using this approximation it is straightforward to estimate the product distribution factors f using Eq. (21) to determine k_{-c} , k_{ae} , and k_{sub} , respectively.

With these approximations we did not expect to reach quantitative agreement. In any instance the RRKM rate coefficients are strongly dependent on the

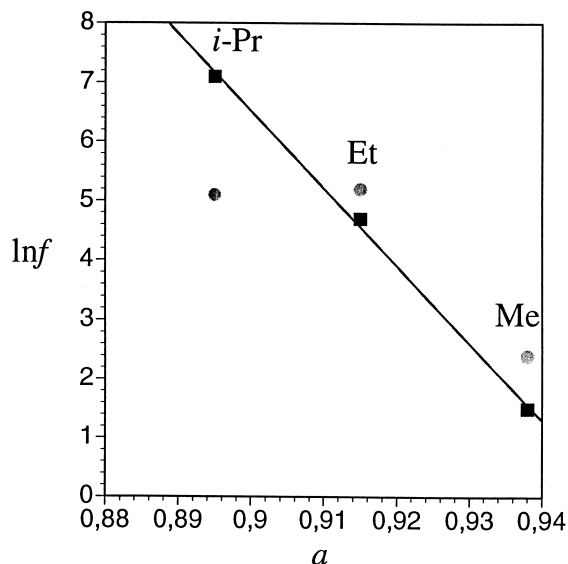


Fig. 3. The natural logarithm of the product distribution factor, $\ln f$, where $f = k_{\text{ae}}/k_{\text{sub}}$, vs. the alkyl group susceptibility constants a . The circles are the experimental data points, whereas the squares are the RRKM values obtained from the MP2 quantum chemical properties (see text). The line is the best fit through the theoretical points.

potential energies of the transition structures, and in principle they are therefore adjustable parameters, at least when quantitatively correct data are unavailable. This is particularly evident from the fact that the importance of the backdissociation reaction, expressed as the ratio $k_{-c}/(k_{-c} + k_{\text{ae}} + k_{\text{sub}})$ appears to be underestimated: 0.00 (CH_3), 0.01 (C_2H_5), 0.09 ($i\text{-C}_3\text{H}_7$), 0.02 ($n\text{-C}_3\text{H}_7$) when compared to the estimated reaction efficiencies reported in Table 1. Although these estimated efficiencies probably have uncertainties of the order of 30%–50%, our judgement is that the relative RRKM rate constants for the back reaction are generally calculated too small. On the other hand, the purpose of these calculation is not to obtain quantitative measures of a rather complicated reaction scheme. By the procedure used here we would instead expect that the trends in reactivity through the two channels **ae** and **sub** should be qualitatively correctly reproduced. We determined the following RRKM (298 K) product distribution f factors: 5 (CH_3), 107 (C_2H_5), 398 ($n\text{-C}_3\text{H}_7$), and 1206 ($i\text{-C}_3\text{H}_7$). No attempt was made to calculate the rates

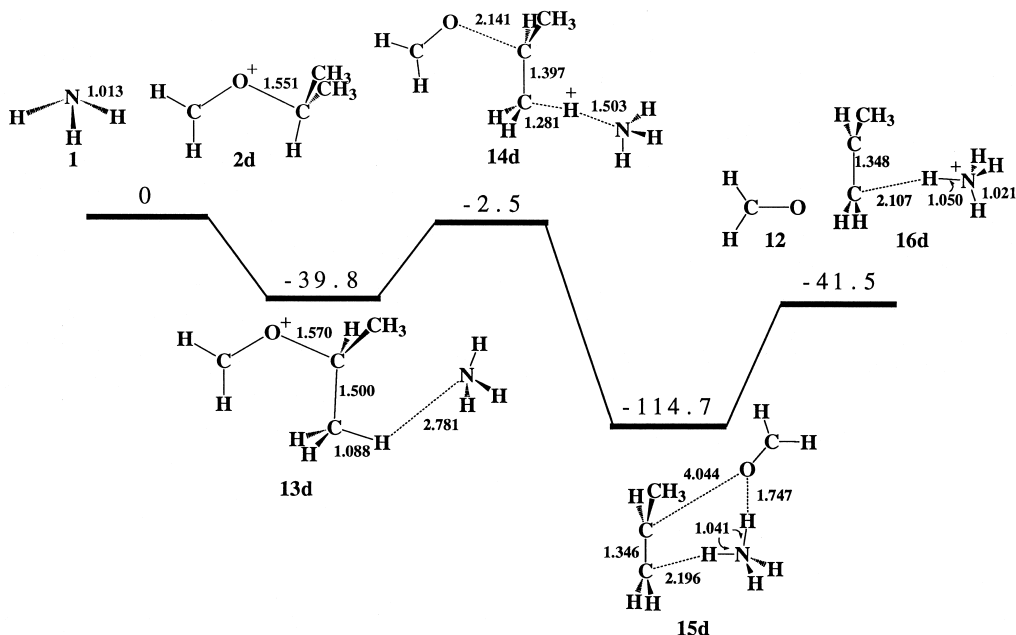
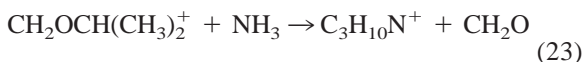


Fig. 4. MP2/6-31G(*d, p*) potential energy diagram for the alternative route for formaldehyde elimination in the reaction between ammonia and the isopropyl oxonium ion. The rate determining step is a proton transfer. Relative energies indicated are in kilojoules per mole and include *zpve* corrections.

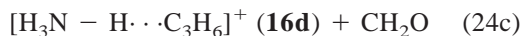
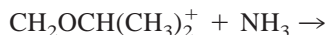
for R = H because the proton transfer does not have a fixed transition structure.

We then plotted the logarithms of the calculated and experimental *f* factors (with exception of *n*-C₃H₇) versus the substituent constants *a* (see previous paragraph for their definition). This is shown in Fig. 3. The three RRKM values fall on a straight line, as we expected, but the experimental points do not. This could of course be the result of imperfections in the MP2 calculations or in the underlying assumptions of the RRKM model used, but could also be the result of a wrong mechanistic interpretation. From the plot it could seem that the point for R = *i*-C₃H₇ represents the exception. The most obvious explanation for this odd behaviour could be that in addition to the anticipated **sub** mechanism, another efficient route for formaldehyde loss is operative:



From our previous experience with S_N2 reactions [48] we have learned that the mechanistic scenarios with

isopropyl and tertiary butyl groups are more intricate than for smaller R groups. In particular reaction routes which includes proton transfer from the alkyl group to the incoming neutral molecule (as, e.g. in an elimination reaction) become more competitive relative to substitution. On this basis we investigated the following candidate mechanism by performing quantum chemical calculations:



It turned out that this mechanism indeed must be of importance. This is shown in Fig. 4. The highest point along the reaction coordinate corresponds to the

transition structure **14d** for the elimination step (24b). This point is only 6 kJ mol⁻¹ higher in energy than TS **9d** of the substitution reaction. The accuracy of this calculated potential energy difference is of course crucial. Only a change by a few kilojoules per mole would result in dramatically different reaction rates from a RRKM calculation. Because the rate determining step of reaction (24) corresponds to a proton transfer, quantum mechanical tunneling [49] is a factor which certainly will enhance its relative importance.

We have compared the MP2 and G2 reaction energies [$E_{\text{ac}}(\text{Prod})$ and $E_{\text{sub}}(\text{Prod})$] with the corresponding experimental values. It turns out that the G2 values on an average are in slightly better agreement than the MP2 values. However, this comparison is severely hampered by the lack of reliable experimental heats of formation, especially for the alkyl oxonium ions. When we compare the MP2 and G2 transition structure energies [$E_{\text{ac}}(\text{TS})$ and $E_{\text{sub}}(\text{TS})$] the overall tendency is that they decrease on going from MP2 to G2, and that the drop for $E_{\text{ac}}(\text{TS})$ is higher than for $E_{\text{sub}}(\text{TS})$. As a consequence, using the G2 barriers in the RRKM calculations instead of the MP2 barriers would lead to a larger deviation from the experimental product distribution factor. This is rather surprising. It should be emphasised though that the performance of the model chemistries G1, G2, and G3 only have been optimised for stable molecular structures, and not for transition structures where bonds are half broken or half formed.

6. Conclusion

The bidentate electrophilic nature of an alkyl oxonium ion is expressed by its reactivity towards ammonia through the observation of two reaction channels: addition/elimination (attack on the carbonyl carbon) and substitution [attack on the sp^3 carbon next to the oxygen (the alpha carbon)]. The competition between the two channels is reproduced by quantum chemical model calculations, which also shows that the potential energy barriers increase with increasing size of the alkyl group. For the most

substituted alkyl group investigated here, *i*-Pr, two different mechanisms contribute to formation of the formal substitution product.

Acknowledgements

The authors wish to thank the Norwegian Research Council (NFR) and VISTA for the grants which made this work possible. The calculations were made possible thanks to support through the NFR Programme for Supercomputing.

References

- [1] R.W. Layer, Chem. Rev. 63 (1963) 489.
- [2] T.H. Lowry, K.S. Richardson, Mechanism and Theory in Organic Chemistry, 2nd ed., Harper & Row, New York, 1981.
- [3] F. Ruff, I.G. Csizmadia, Organic Reactions: Equilibria, Kinetics and Mechanism, Elsevier, Amsterdam, 1994.
- [4] W.P. Jencks, J. Am. Chem. Soc. 81 (1959) 475.
- [5] W.P. Jencks, Chem. Rev. 72 (1972) 705.
- [6] A. Maquestiau, R. Flammang, L. Nielsen, Org. Mass Spectrom. 15 (1980) 376.
- [7] J.C. Tabet, D. Fraisse, Org. Mass Spectrom. 16 (1981) 45.
- [8] D.J. Burinsky, J.E. Campana, R.G. Cooks, Int. J. Mass Spectrom. Ion Processes 62 (1984) 303.
- [9] M. Pykäläinen, A. Vainiotalo, T. Pakkanen, P. Vainiotalo, J. Mass Spectrom. 31 (1996) 716.
- [10] J.K. Pau, J.K. Kim, M.C. Caserio, J. Am. Chem. Soc. 100 (1978) 3838.
- [11] S. Okada, Y. Abe, S. Taniguchi, S. Yamabe, J. Am. Chem. Soc. 109 (1987) 295.
- [12] M.T. Kinter, M.M. Bursley, J. Am. Chem. Soc. 108 (1986) 1797.
- [13] J.K. Pau, J.K. Kim, M.C. Caserio, J. Am. Chem. Soc. 100 (1978) 3831.
- [14] I.H. Williams, D. Spangler, D.A. Femec, G.M. Maggiora, R.L. Schowen, J. Am. Chem. Soc. 102 (1980) 6619.
- [15] J.C. Sheldon, G.J. Currie, J.H. Bowie, Aust. J. Chem. 39 (1986) 839.
- [16] Z. Karpas, M. Meot-Ner, J. Phys. Chem. 93 (1989) 1859.
- [17] I.A. Williams, L'Actualité Chimique 1991 (Jan/Feb 1999) 27.
- [18] O.N. Ventura, E.L. Cotiño, A. Lledós, J. Bertran, J. Comp. Chem. 13 (1992) 1037.
- [19] H.E. Audier, T.B. McMahon, J. Mass Spectrom. 32 (1997) 201.
- [20] G. van der Rest, P. Mourgues, J. Fossey, H.E. Audier, Int. J. Mass Spectrom. Ion Processes 160 (1997) 107.
- [21] G. van der Rest, G. Bouchoux, H.E. Audier, T.B. McMahon, Eur. Mass Spectrom. 4 (1998) 339.
- [22] M.A. Freitas, R.A.J. O'Hair, Int. J. Mass Spectrom. Ion Processes 175 (1998) 107.

- [23] M.C. Caserio, J.K. Kim, *J. Org. Chem.* 47 (1982) 2940.
- [24] R. van Doorn, N.M.M. Nibbering, *Org. Mass Spectrom.* 13 (1978) 527.
- [25] J.K. Kim, J. Bonicamp, M.C. Caserio, *J. Org. Chem.* 46 (1981) 4230.
- [26] R.C. Dunbar, J. Shen, E. Melby, G.A. Olah, *J. Am. Chem. Soc.* 95 (1973) 7200.
- [27] H.E. Audier, T.B. McMahon, *J. Am. Chem. Soc.* 116 (1994) 8294.
- [28] P.F. Wilson, M.J. McEwan, M. Meot-Ner, *Int. J. Mass Spectrom. Ion Processes* 132 (1994) 149.
- [29] E.S. Eichmann, J.S. Brodbelt, *J. Am. Soc. Mass Spectrom.* 4 (1993) 97.
- [30] E.S. Eichmann, J.S. Brodbelt, *J. Am. Soc. Mass Spectrom.* 4 (1993) 230.
- [31] E. Uggerud, *J. Chem. Soc., Perkin Trans. 2* 1996 (1996) 1915.
- [32] L.J. de Koning, N.M.M. Nibbering, S.L. van Orden, F.H. Laukien, *Int. J. Mass Spectrom. Ion Processes* 165/166 (1997) 209.
- [33] Y. Ikezoe, S. Matsuoka, M. Takebe, A. Viggiano, *Gas Phase Ion–Molecule Reaction Rate Constants Through 1986*, Maruzen, Tokyo, 1987.
- [34] T. Su, W. Chesnavich, *J. Chem. Phys.* 76 (1982) 5183.
- [35] M.J. Frisch, G.W. Trucks, H.B. Schlegel, P.M.W. Gill, B.G. Johnson, M.A. Robb, J.R. Cheeseman, T.A. Keith, G.A. Peterson, J.A. Montgomery, K. Raghavachari, M.A. Al-Laham, V.G. Zakrzewski, J.V. Ortiz, J.B. Foresman, J. Cioslowski, B.B. Stefanov, A. Nanayakkara, M. Challacombe, C.Y. Peng, P.Y. Ayala, W. Chen, M.W. Wong, J.L. Andres, E.S. Replogle, R. Gomperts, R.L. Martin, D.J. Fox, J.S. Binkley, D.J. Defrees, J. Baker, J.J.P. Stewart, M. Head-Gordon, C. Gonzalez, J.A. Pople, *GAUSSIAN 94*, M.J. Frisch, G.W. Trucks, H.B. Schlegel, P.M.W. Gill, B.G. Johnson, M.A. Robb, J.R. Cheeseman, T.A. Keith, G.A. Peterson, J.A. Montgomery, K. Raghavachari, M.A. Al-Laham, V.G. Zakrzewski, J.V. Ortiz, J.B. Foresman, J. Cioslowski, B.B. Stefanov, A. Nanayakkara, M. Challacombe, C.Y. Peng, P.Y. Ayala, W. Chen, M.W. Wong, J.L. Andres, E.S. Replogle, R. Gomperts, R.L. Martin, D.J. Fox, J.S. Binkley, D.J. Defrees, J. Baker, J.J.P. Stewart, M. Head-Gordon, C. Gonzalez, J.A. Pople (Eds.) *Gaussian Inc., Pittsburgh, PA*, 1994.
- [36] M.J. Frisch, J.A. Pople, J.S. Binkley, *J. Chem. Phys.* 80 (1984) 3265.
- [37] C.C.J. Roothan, *Rev. Mod. Phys.* 23 (1951) 69.
- [38] C. Möller, M.S. Plesset, *Phys. Rev.* 46 (1934) 618.
- [39] L.A. Curtiss, K. Raghavachari, G.W. Trucks, J.A. Pople, *J. Chem. Phys.* 94 (1991) 7221.
- [40] A.P. Scott, L. Radom, *J. Phys. Chem.* 100 (1996) 16502.
- [41] R.G. Gilbert, S.C. Smith, *Theory of Unimolecular and Recombination Reactions*, Blackwell Scientific, Oxford, 1990.
- [42] A. Matsumoto, S. Okada, S. Taniguchi, T. Hayakawa, *Bull. Chem. Soc. Jpn.* 48 (1975) 3387.
- [43] D. Smith, *Chem. Rev.* 92 (1992) 1473.
- [44] E. Herbst, *Annu. Rev. Phys. Chem.* 46 (1995) 27.
- [45] G. Bouchoux, Y. Hoppilard, *Int. J. Mass Spectrom. Ion Processes* 75 (1987) 1.
- [46] E. Uggerud, for a given alkyl group the factor a is the slope of the straight line obtained when the alkyl cation affinity for a variety of substances is plotted with respect to the proton affinity, unpublished.
- [47] J.R. Murdoch, *J. Am. Chem. Soc.* 94 (1972) 4410.
- [48] E. Uggerud, L. Bache-Andreassen, *Chem. Eur. J.* 5 (1999) 1917.
- [49] R.P. Bell, *The Proton in Chemistry*, 2nd ed., Chapman and Hall, London, 1973.